Physica E 71 (2015) 21–30

Contents lists available at ScienceDirect

Physica E

journal homepage: www.elsevier.com/locate/physe

A variational size-dependent model for electrostatically actuated NEMS incorporating nonlinearities and Casimir force

Binbin Liang [a], Long Zhang [a], Binglei Wang [a,b,*], Shenjie Zhou [c]

[a] School of Civil Engineering, Shandong University, Jinan 250061, China
[b] State Key Laboratory for Strength and Vibration of Mechanical Structures, School of Aerospace, Xi'an Jiaotong University, Xi'an 710049, China
[c] School of Mechanical Engineering, Shandong University, Jinan 250061, China

HIGHLIGHTS

- A variational size-dependent model for the electrostatically actuated NEMS is presented.
- The model incorporates nonlinearities and Casimir force.
- The results reveal that Casimir force can reduce the external applied voltage.
- Pull-in instability may occur without applied voltage due to Casimir force.
- Size effect and Casimir force should be considered for precisely modeling NEMS.

ARTICLE INFO

Article history:
Received 5 November 2014
Received in revised form
16 March 2015
Accepted 27 March 2015
Available online 28 March 2015

Keywords:
Casimir force
Detachment length
Minimum gap
Size effect
NEMS

ABSTRACT

A size-dependent model for the electrostatically actuated Nano-Electro-Mechanical Systems (NEMS) incorporating nonlinearities and Casimir force is presented by using a variational method. The governing equation and boundary conditions are derived with the help of strain gradient elasticity theory and Hamilton principle. Generalized differential quadrature (GDQ) method is employed to solve the problem numerically. The pull-in instability with Casimir force included is then studied. The results reveal that Casimir force, which is a spontaneous force between the two electrodes, can reduce the external applied voltage. With Casimir force incorporated, the pull-in instability occurs without voltage applied when the beam size is in nanoscale. The minimum gap and detachment length can be calculated from the present model for different beam size, which is important for NEMS design. Finally, discussions of size effect induced by the strain gradient terms reveal that the present model is more accurate since size effect play an important role when beam in nanoscale.

1. Introduction

Rapid progress in device miniaturization has led to the quick rise of Nano-Electro-Mechanical Systems (NEMS) due to the many advantages such as fast response, low energy consumption and low cost [1]. Nanobeam models subjected to electrostatic force are typically introduced in various kinds of NEMS such as nano-switch [2], nano-resonators and nano-pressure sensors [3].

A typical electrostatically actuated NEMS includes two parts: a fixed electrode and a conductive deformable electrode (Fig. 1). An applied voltage between the two electrodes results in the deflection of the deformable electrode due to electrostatic attraction, and a subsequent change in the system capacitance. When the voltage increases beyond a critical value, the movable electrode becomes unstable and collapses onto the fixed electrode, which is called the pull-in instability phenomenon. The critical displacement and the critical voltage associated with this instability are referred to as the pull-in displacement and the pull-in voltage, respectively. Such pull-in instability is a saddle-node bifurcation, which exhibits snap-through phenomenon [4]. Some applications including nano-resonators and nano-pressure sensors should avoid such instability in order to achieve stable operations and maximize device sensitivity; whereas some other applications such as optical/RF switches are underpinned by the pull-in instability, where it is critical to fine-tune the critical voltage so that the switch on and off functions can be well-controlled. Hence, the accurate modeling of the static and dynamic bending behavior of nanobeams seems to be crucial in order to study the mechanical

* Corresponding author at: School of Civil Engineering, Shandong University, Jinan 250061, China.
E-mail address: bwang@sdu.edu.cn (B. Wang).

http://dx.doi.org/10.1016/j.physe.2015.03.020
1386-9477/

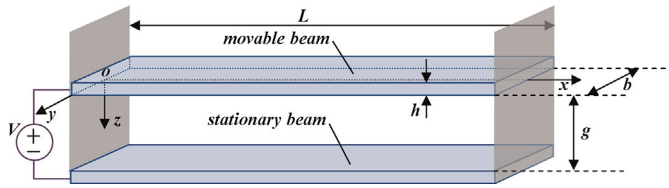

Fig. 1. Schematic of a fixed–fixed NEMS.

and electric behaviors of these NEMS.

In general, the characteristic size of these nanobeams are comparable to the material microstructure, e.g., the grain size or atomic lattice spacing, which leads to distinct mechanical and electric behaviors with respect to their macroscopic counterparts. Numerous experiments have observed the size-dependent behaviors in metals [5, 6], brittle materials [7], polymers [8, 9] and polysilicon [10]. These behaviors cannot be explained by the classical continuum theory, which does not have material length scale parameter (MLSP).

Among the size dependent continuum theories, the nonlocal theory [11], the surface energy theory [12], the modified couple stress theory [13] and strain gradient elasticity theory [8] are proposed to predict the size-dependent phenomena. When applying the nonlocal theory, a paradoxical conclusion arises in some cases. For example, the small length-scale effect vanishes in the bending deflection for the Euler–Bernoulli cantilever nanobeam under a transverse point load. Moreover, the nonlocal theory predicts a "softening effect", which is inconsistent with the "stiffening effect" observed in experiments. For surface energy theory, it is considered that the surface properties cannot be overlooked in the study of nanostructures and nanomaterials due to the large value of surface to volume ratios at that scale [14]. Although it is applied to study the size dependent behaviors, it is had to admit that the fundamental properties are not only relative to the surface part but also relative to the internal part because the characteristic length is in the bulk such as the grain size or atomic lattice spacing. With only one MLSP incorporated, the modified couple stress theory [13] are also been used to predict the size dependent phenomenon [15–17], which is a special case of the strain gradient elasticity theory suggested by Lam et al. [8]. Strain gradient elasticity theory has been applied to study the linear [18] and nonlinear [19] Euler beam, linear [20] and nonlinear [21] Timoshenko beam and Reddy–Levinson beam [22], and is also employed to investigate the size-dependent pull-in phenomena in MEMS [23–25].

With the decrease in device dimensions from the micro- to nanoscale, additional forces on NEMS, such as the Casimir force, should be considered. The Casimir force represents the attraction of two uncharged material bodies due to modification of the zero-point energy associated with the electromagnetic modes in the space between them [26]. During the manufacturing, the movable electrode in NEMS device collapses and sticks on fixed electrode, if the distance between each other become less enough to critical value or the lengths longer than critical lengths [27]. The two critical values referred to the minimum initial gap and the detachment length [28], respectively. Therefore, the existence of the Casimir force poses a severe constraint on the miniaturization of electrostatically actuated devices. The Casimir interaction is proportional to the inverse fourth power of the distance of separation. Batra et al. [26,29,30] have studied the pull-in instability in micromembrane, rectangular, circular and elliptic plates incorporating Casimir force. The saddle–node bifurcation behavior of nanoscale electrostatic actuators considering the Casimir force and the effect of Casimir force on the pull-in parameters were studied [27,31], and an approximate analytical expression of the critical pull-in gap was obtained by the perturbation theory. Not only Casimir force but also geometric nonlinearity are considered in some studies, such as electrostatically actuated von Karman circular by Wang et al. [32], micro-switch by Jia et al. [33].

Unfortunately these works are based on the classical continuum theory, which cannot capture the size effect in micro-/nano-scale. In our previous works, strain gradient theory is introduced to study the size dependent pull-in instability of electrostatically actuated beam and plate without considering the Casimir force [23–25]. For nanoscale structures in NEMS which will be studied in the present paper, the nonlinearities and Casimir force together with strain gradient terms are considered simultaneously here, which is the main gap we attempt to bridge in the present paper.

The rest of the paper is organized as follows. In Section 2, the theoretical formulations are derived based on a variational procedure. A generalized differential quadrature (GDQ) method is employed to analyze the higher order differential equation and numerical results and discussions are presented in Section 3. Finally some concluding remarks are summarized in Section 4.

2. Theoretical formulations

2.1. Strain gradient elasticity theory

Based on the assumptions of strain gradient elasticity theory [8], the bending strain energy U_m in a deformed isotropic linear elastic material occupying region Ω (with a volume element V) is given by

$$U_m = \frac{1}{2}\int_{\Omega} u_m \, dV = \frac{1}{2}\int_{\Omega} (\sigma_{ij}\varepsilon_{ij} + p_i \gamma_i + \tau^{(1)}_{ijk}\eta^{(1)}_{ijk} + m^s_{ij}\chi^s_{ij})dV \tag{1}$$

in which, u_m is the strain energy density. The Cauchy stress tensor (σ_{ij}) and the higher-order stress tensors (p_i,$\tau^{(1)}_{ijk}$, and m^s_{ij}) are conjugated with the strain tensor (ε_{ij}) and three strain gradient tensors: the dilatation gradient tensor, γ_i, the deviatoric stretch gradient tensor,$\eta^{(1)}_{ijk}$, and the symmetric rotation gradient tensor,χ^s_{ij},via

$$\sigma_{ij} = \frac{\partial u_m}{\partial \varepsilon_{ij}}, \quad p_i = \frac{\partial u_m}{\partial \gamma_i}, \quad \tau^{(1)}_{ijk} = \frac{\partial u_m}{\partial \eta^{(1)}_{ijk}}, \quad m^s_{ij} = \frac{\partial u_m}{\partial \chi^s_{ij}} \tag{2}$$

where the strain energy density is a function of the strain and the strain gradient metrics.

With the displacement field is given, the strain and strain gradient tensors are defined by

$$\varepsilon_{ij} = \frac{1}{2}(\partial_j u_i + \partial_i u_j) \tag{3}$$

$$\gamma_i = \partial_i \varepsilon_{mm} \tag{4}$$

$$\eta^{(1)}_{ijk} = \eta^s_{ijk} - \frac{1}{5}(\delta_{ij}\eta^s_{mmk} + \delta_{jk}\eta^s_{mmi} + \delta_{ki}\eta^s_{mmj}) \tag{5}$$

and

$$\chi^s_{ij} = \frac{1}{4}(e_{ipq}\partial_p\varepsilon_{qj} + e_{jpq}\partial_p\varepsilon_{qi}) \tag{6}$$

where ∂_i is the differential operator, u_i is the displacement vector, ε_{mm} is the dilatation strain, and η^s_{ijk} is the symmetric part of second order displacement gradient tensor defined by,

$$\eta^s_{ijk} = \frac{1}{3}(u_{i,jk} + u_{j,ki} + u_{k,ij}) \tag{7}$$

δ_{ij} and e_{ijk} are the Kronecker symbol and the alternate symbol, respectively. Here, it should be noted that the index notation will always be used with repeated indices denoting summation from (1)–(3).

The corresponding stress tensors, respectively, are given by the following constitutive relations,

$$\sigma_{ij} = k\delta_{ij}\varepsilon_{mm} + 2\mu\varepsilon'_{ij} \tag{8}$$

$$p_i = 2\mu l_0^2\gamma_i \tag{9}$$

$$\tau_{ijk}^{(1)} = 2\mu l_1^2\eta_{ijk}^{(1)} \tag{10}$$

$$m_{ij}^s = 2\mu l_2^2\chi_{ij}^s \tag{11}$$

where ε'_{ij} is the deviatoric strain defined as

$$\varepsilon'_{ij} = \varepsilon_{ij} - \frac{1}{3}\varepsilon_{mm}\delta_{ij} \tag{12}$$

k and μ are bulk and shear modules, respectively, l_0, l_1, and l_2 are the additional independent MLSPs associated with the dilatation gradients, deviatoric stretch gradients and symmetric rotation gradients, respectively. As mentioned by Lam [8], three independent material length scale parameters are internal parameters for a given material, which only can be determined from uniaxial tensile or compressive, bending or torsion experiments for different size. It is noted that the strain gradient elasticity theory will reduce to the modified couple stress theory [13] if $l_0=l_1=0$; and it will further reduce to the classical continuum theory if $l_0=l_1=l_2=0$.

2.2. The variational size-dependent model

The nonlinear governing equation of a nanobeam with immovable supports as well as all boundary conditions can be derived with the help of the strain gradient elasticity theory and Hamilton's principle (Variational approach).

According to Hamilton's principle, the actual motion minimizes the difference of the kinetic energy and total potential energy for a system with prescribed configurations at t_1 and t_2. That is

$$\delta\int_{t1}^{t2}[T-(U_m+U_s-W-U_e-U_c)]dt=0 \tag{13}$$

in which, U_m and U_s are, respectively, the bending strain energy and energy due to axial forces stored in the deformed beam. T is kinetic energy, W the work done by external forces, U_e and U_c are the electrostatic potential energy and the Casimir effect energy between the two electrodes, respectively.

Consider a straight beam subjected to a static lateral load $q(x)$ distributed along the longitudinal axis x of the beam, as shown in Fig. 1. The loading plane coincides with the xz plane, and the cross-section of the beam parallels to the yz plane.

Based on the Bernoulli–Euler beam assumption, the bending strain energy (Eq. (1)), with strain gradient incorporated, is expressed by [18]

$$U_m=\frac{1}{2}\int_0^L D_1\left(\frac{\partial^2 w}{\partial x^2}\right)^2dx+\frac{1}{2}\int_0^L D_2\left(\frac{\partial^3 w}{\partial x^3}\right)^2dx \tag{14}$$

in which

$$D_1 = EI + 2\mu Al_0^2 + \frac{8}{15}\mu Al_1^2 + \mu Al_2^2 D_2 = 2\mu Il_0^2 + \frac{4}{5}\mu Il_1^2 \tag{15}$$

and x is the position along the beam length, w is bending displacement. A and I are the area and moment of inertia of the cross section, E is Young's modulus. μ is shear modulus, l_0, l_1 and l_2 are the independent material length scale parameters (MLSPs) associated with the dilatation gradients, deviatoric stretch gradients, and symmetric rotation gradients, respectively.

The energy U_s stored in the beam due to axial forces is

$$U_s=-\frac{1}{4}\int_0^L(2N_0+N_s)\left(\frac{\partial w}{\partial x}\right)^2dx \tag{16}$$

N_0 is positive or negative depending on either a tensile or compressive axial applied load or residual force expressed by $N_0=\bar{\sigma}A$ with $\bar{\sigma}$ the residual stress. N_s is the additional axial force associated with the mean axial extension of the beam.

$$N_s=\frac{EA}{2L}\int_0^L\left(\frac{\partial w}{\partial x}\right)^2dx \tag{17}$$

The kinetic energy T of the beam has the form

$$T=\frac{1}{2}\int_0^L\rho A\left(\frac{\partial w}{\partial t}\right)^2dx \tag{18}$$

where t is the time, ρ is the material density.

And the work W done by the externally transverse force, $q(x)$, the boundary shear force $\bar{Q}$, the boundary classical bending moments $\bar{M}$ and the higher bending moment $\bar{M}^h$, respectively, may be written as

$$W=\int_0^L q(x)w(x)dx+[\bar{Q}w]\Big|_0^L+[\bar{M}w']|_0^L+[\bar{M}^h w'']\Big|_0^L \tag{19}$$

The electrostatic potential energy U_e, which is the summation of the electrostatic energy stored between the upper and lower electrodes of the plate and the electrostatic energy of the voltage source, is given by

$$U_e=\frac{\varepsilon bV^2}{2}\int_0^L\left(\frac{1}{(d-w)}+\frac{2}{\pi b}\ln\left(\frac{1}{d-w}\right)\right)dx \tag{20}$$

in which, $\varepsilon = 8.854\times10^{-12}\,C^2N^{-1}m^{-2}$ is the dielectric constant of the gap medium. V is applied voltage between two electrodes.

In quantum field theory, the Casimir effect is physical forces arising from a quantized field. And in applied physics, the Casimir effect plays an important role in some aspects of emerging microtechnologies and nanotechnologies. The Casimir effect energy between the two electrodes is

$$U_c=\int_0^L\frac{\hbar c\pi^2 b}{720(d-w)^3}dx \tag{21}$$

where $\hbar = 1.055\times10^{-34}\,J\cdot s$ is Planck's constant divided by 2π and c the speed of light in vacuum.

Substituting Eqs. (14), (16), (18)–(21) into Hamilton's principle Eq. (13), after somewhat lengthy but straightforward manipulations, it takes the following form

$$\begin{aligned}
&\int_{t1}^{t2}\int_0^L\Bigg(-D_2\frac{\partial^6 w}{\partial x^6}+D_1\frac{\partial^4 w}{\partial x^4}+\rho A\frac{\partial^2 w}{\partial t^2}\\
&\quad-\left[\frac{EA}{2l}\int_0^l\left(\frac{\partial w}{\partial x}\right)^2dx+N_0\right]\frac{\partial^2 w}{\partial x^2}-q-F_e-F_c\Bigg)\delta w dx dt\\
&\quad+\int_{t1}^{t2}\left[(\bar{Q}-D_1\frac{\partial^3 w}{\partial x^3}+D_2\frac{\partial^5 w}{\partial x^5})\delta w\Big|_0^L\right]dt\\
&\quad+\int_{t1}^{t2}\left[(\bar{M}+D_1\frac{\partial^2 w}{\partial x^2}-D_2\frac{\partial^4 w}{\partial x^4})\delta(\frac{\partial w}{\partial x})\Big|_0^L\right]dt\\
&\quad+\int_{t1}^{t2}\left[(\bar{M}_h+D_2\frac{\partial^3 w}{\partial x^3})\delta(\frac{\partial^2 w}{\partial x^2})\Big|_0^L\right]dt\\
&=0
\end{aligned} \tag{22}$$

in which

$$F_e=\frac{\bar{\varepsilon}bV^2}{2(d-w)^2}(1+\frac{2}{\pi}\frac{d-w}{b}) \tag{23}$$

$$F_c = \frac{\hbar c \pi^2 b}{240(d+w)^4} \tag{24}$$

Due to the variational principle for arbitrary δw, the governing equation is finally obtained:

$$-D_2\frac{\partial^6 w}{\partial x^6} + D_1\frac{\partial^4 w}{\partial x^4} + \rho bh\frac{\partial^2 w}{\partial t^2} - \left[\frac{EA}{2l}\int_0^l \left(\frac{\partial w}{\partial x}\right)^2 dx + N_0\right]\frac{\partial^2 w}{\partial x^2} = q(x) + F_e + F_c \tag{25}$$

in which *q(x)* represents the external distributed force, F_e and F_c represent the electrostatic force and Casimir force between two electrodes assuming that the area between the nanobeam and the stationary electrode completely overlaps.

With $q(x)=0$ in Eq. (25), the nanobeam excited by the electroelastic force and the Casimir force is theoretically governed by the following equation:

$$-D_2\frac{\partial^6 w}{\partial x^6} + D_1\frac{\partial^4 w}{\partial x^4} + \rho bh\frac{\partial^2 w}{\partial t^2} - \left[\frac{EA}{2l}\int_0^l \left(\frac{\partial w}{\partial x}\right)^2 dx + N_0\right]\frac{\partial^2 w}{\partial x^2} = F_e + F_c \tag{26}$$

The corresponding boundary conditions at the edges can also be obtained from Eq. (22):

$$\left[\bar{Q} - D_1\frac{\partial^3 w}{\partial x^3} + D_2\frac{\partial^5 w}{\partial x^5}\right]_{x=0,L} = 0 \quad \text{or} \quad w\Big|_{x=0,L} = 0 \tag{27}$$

$$\left[\bar{M} + D_1\frac{\partial^2 w}{\partial x^2} - D_2\frac{\partial^4 w}{\partial x^4}\right]_{x=0,L} = 0 \quad \text{or} \quad \frac{\partial w}{\partial x}\Big|_{x=0,L} = 0 \tag{28}$$

$$\left[\bar{M}_h + D_2\frac{\partial^3 w}{\partial x^3}\right]_{x=0,L} = 0 \quad \text{or} \quad \frac{\partial^2 w}{\partial x^2}\Big|_{x=0,L} = 0 \tag{29}$$

Eqs. (27) and (28) are the classical boundary conditions and Eq. (29) is the non-classical boundary conditions. The first equations in Eqs. (27)–(29) are the natural boundary conditions; and the second ones in Eqs. (27)–(29) are the kinematic end conditions [34].

For the fixed–fixed nanobeam, the classical boundary conditions are easily determined:

$$w = 0, \quad \frac{\partial w}{\partial x} = 0, \quad \text{for} \quad x = 0, L \tag{30}$$

The non-classical boundary conditions are determined either from the natural boundary conditions or the kinematic end conditions in Eq. (29).

$$\bar{M}_h + D_2\frac{\partial^3 w}{\partial x^3} = 0 \quad \text{or} \quad \frac{\partial^2 w}{\partial x^2} = 0 \quad \text{for } x = 0, L \tag{31}$$

Generally, for the higher-order strain gradient theory, the higher moment ($\bar{M}_h$) is not yet given. Therefore, $\partial^2 w/\partial x^2 = 0$ (for $x = 0, L$) is used as the non-classical boundary conditions.

Thus, all the boundary conditions are

$$w = 0, \quad \frac{\partial w}{\partial x} = 0, \quad \frac{\partial^2 w}{\partial x^2} = 0 \quad \text{for } x = 0, L \tag{32}$$

The nanobeam excited by the electroelastic force and the Casimir force is governed by Eq. (26) with $q(x) = 0$ and the boundary conditions (32).

If neglecting the Casimir force and l_0, l_1 are set to be zero, the governing Eq. (25) will reduce to that of Ref. [35] which is based on the modified couple stress theory [13]. Furthermore, when the MLSPs are ignored (i.e. $l_0=l_1=l_2=0$), the sixth-order term in the governing Eq. (26) vanishes and the non-classical equation in the boundary condition Eq. (32) vanishes; in that case, the present model with size effect can be reduced to the classical model [36].

3. Numerical analysis with GDQ method

3.1. GDQ method and its application

Shu and Richards [37] proposed the GDQ method to numerically solve PDEs using considerably fewer grid points. This method is based on the idea that the derivative of a function with respect to a coordinate can be expressed as a weighted linear summation of function values at all mesh points along that direction. Here we briefly summarize the results of one-dimensional problems and for more details of the GDQ method, one may refer to Ref. [38].

The *N*-th order derivative of a function $w(x)$ with respect to x in the overall domain is approximated as:

$$w(x) = \sum_{j=1}^{N} w(x_j) g_j(x) \tag{33}$$

where $g_i(x)$ are the Lagrange interpolated polynomials of equations, and N is the total number of grid points in the computational domain [39, 40], that is

$$g_j(x) = \frac{M(x)}{(x - x_j)M^{(1)}(x_j)} \tag{34}$$

with

$$M(x) = \prod_{k=1}^{N}(x - x_k), \quad M^{(1)}(x_j) = \prod_{k=1,k\neq j}^{N}(x_j - x_k) \tag{35}$$

And x_i are the shifted Chebyshev–Gauss–Lobatto nodes, defined as:

$$x_i = \frac{1}{2}\left(1 - \cos\frac{i-1}{N-1}\pi\right), \quad i = 1, 2, \ldots, N \tag{36}$$

The *m*th-order derivative of a function *w(x)* at the *i*-th point, x_i, is approximated as

$$w^{(m)}(x_i) = \sum_{j=1}^{N} c_{ij}^{(m)} w(x_i), \quad i = 1, 2, \ldots, N \tag{37}$$

where $w^{(m)}(x_i)$ is the m-th order derivative of $w(x)$ at x_i. $c_{ij}^{(m)}$ is the weighting factor for the approximation of the *m*-th order derivative of the *i*-th point.

Thus, the first order weighting factor $c_{ij}^{(1)}$ $(i, j = 1, 2, \ldots, N)$ can be obtained analytically from the differentiation of Eq. (34), i.e.,

$$c_{ij}^{(1)} = M^{(1)}(x_i)/(x_i - x_j)M^{(1)}(x_j) \quad \text{for} \quad i \neq j, \quad i = 1, 2, \ldots, N c_{ii}^{(1)} = -\sum_{\substack{j=1\\ j\neq i}}^{N} c_{ij}^{(1)} 3 \text{ for } i = 1, 2, \ldots, N \tag{38}$$

The weighting coefficients for the second and higher-order derivatives can be obtained similarly. The following recurrence relationship can be found for the *m*-th order weighting factors: $c_{ij}^{(m)}$

$$c_{ij}^{(m)} = m(c_{ii}^{(m-1)}c_{ij}^{(1)} - \frac{c_{ij}^{(m-1)}}{x_i - x_j}) \text{ for } i \neq j, m = 2, 3, \ldots, N-1, \quad i, j = 1, 2, \ldots, N c_{ii}^{(m)} = -\sum_{j=1, j\neq i}^{N} c_{ij}^{(m)} \text{ for } i = 1, 2, \ldots, N \tag{39}$$

To solve the governing Eq. (26) with boundary conditions Eq. (32), the nondimensional variables (denoted with hats) are introduced,

$$\hat{w} = \frac{w}{d}, \quad \hat{x} = \frac{x}{L}, \quad \hat{t} = \frac{t}{T} \tag{40}$$

where T is a time scale defined below. Substituting Eq. (40) into Eqs. (26) and (32) and remove the hats, we obtain

$$\alpha_0\frac{\partial^6 w}{\partial x^6} + \frac{\partial^4 w}{\partial x^4} + \frac{\partial^2 w}{\partial t^2} - \left[\alpha_1\int_0^1 (\frac{\partial w}{\partial x})^2 dx + N\right]\frac{\partial^2 w}{\partial x^2} = \alpha_2 V^2\left(\frac{1}{(1-w)^2} + \frac{f}{1-w}\right) + \frac{\alpha_3}{(1-w)^4} \tag{41}$$

with

$$\alpha_0 = -\frac{D_2}{D_1 L^2}; \quad \alpha_1 = \frac{EAd^2}{2D_1}; \quad \alpha_2 = \frac{\varepsilon b L^4}{2D_1 d^3}; \quad f = \frac{2d}{\pi b}$$
$$\alpha_3 = \frac{\hbar c\pi^2 b L^4}{240 D_1 d^5}; \quad N = \frac{L^2}{D_1}N_0; \quad T^2 = \frac{\rho A L^4}{D_1} \tag{42}$$

and the corresponding boundary conditions are

$$w(0) = 0; \quad \frac{\partial w(0)}{\partial x} = 0; \quad \frac{\partial^2 w(0)}{\partial x^2} = 0$$
$$w(1) = 0; \quad \frac{\partial w(1)}{\partial x} = 0; \quad \frac{\partial^2 w(1)}{\partial x^2} = 0 \tag{43}$$

For the static problem, the time derivatives in Eq. (41) are set to zero, and electric voltage is assumed to be constant. Then, Eq. (41) is rewritten as:

$$\alpha_0\frac{\partial^6 w}{\partial x^6} + \frac{\partial^4 w}{\partial x^4} - \left[\alpha_1\int_0^1 (\frac{\partial w}{\partial x})^2 dx + N\right]\frac{\partial^2 w}{\partial x^2} = \alpha_2 V^2\left(\frac{1}{(1-w)^2} + \frac{f}{1-w}\right) + \frac{\alpha_3}{(1-w)^4} \tag{44}$$

for any $x \in [0, 1]$.

By solving Eq. (44) satisfied with boundary conditions (43), the static deformation $w(x)$ may be determined.

With GDQ method is applied, the governing Eq. (44) is rewritten in the following discrete form.

$$\alpha_0(c_{ij}^{(6)}w_j) + c_{ij}^{(4)}w_j - \left[\alpha_1\sum_{k=1}^{N} C_k\left(c_{ij}^{(1)}w_j(x_k)\right)^{\circ 2} + N\right](c_{ij}^{(2)}w_j) = \alpha_2 V^2\left[f_1^{\circ}(w_j) + f_2^{\circ}(w_j)\right] + \alpha_3 f_3^{\circ}(w_j) \tag{45}$$

in which $i, j = 1, 2, \cdots, N$ and

$$f_1(x) = \frac{1}{(1-x)^2} \quad f_2(x) = \frac{f}{1-x} \quad f_3(x) = \frac{1}{(1-x)^4} \tag{46}$$

and '∘' is the Hadamard matrix product [41]. C_k is derived using the Newton–Cotes integration [42]:

$$C_k = \int_0^1 \prod_{\substack{i=1 \\ i\neq k}}^{N} \frac{x - x_i}{x_k - x_i} dx \tag{47}$$

Furthermore, the boundary conditions in Eq. (43) may be written as

$$w_1 = 0; \qquad w_N = 0$$
$$\sum_{j=1}^{N} e_{1j}^{(1)}w_j = 0; \quad \sum_{j=1}^{N} e_{Nj}^{(1)}w_j = 0$$
$$\sum_{j=1}^{N} e_{1j}^{(2)}w_j = 0; \quad \sum_{j=1}^{N} e_{Nj}^{(2)}w_j = 0 \tag{48}$$

By substituting Eq. (48) into Eq. (45), the static problem of a electrostatically actuated micro-beam can be solved numerically. The pseudo-arclength algorithm is applied to iterate the discrete equation [43]. The natural frequencies of the device can be obtained by taking the square root of the magnitudes of the individual eigenvalues, which is deduced from the Jacobian matrix of Eq. (45) for a given voltage.

3.2. Numerical results and discussion

The newly developed model and solution algorithm are subsequently employed to study the size-dependent pull-in instability of nanobeam-based NEMS devices under a constant DC loading; especially the effects of Casmir force and strain gradient on the pull-in phenomena are discussion.

3.2.1. Pull-in instability

Firstly, the new model is introduced to study the pull-in instability by illustrating the relationship between the mid-point nondimensional displacement, w_{max}, and applied voltage, which are shown in Fig. 2. In the calculation, the geometrical and material properties of the system are L=210 μm, b=100 μm, h=1.5 μm, d=1.18 μm, E=151 Gpa and ν=0.3. For simplication, here and what follow in the rest paper, the material length scale parameters are assumed the same, i.e. $l_0=l_1=l_2=Cl$. Here Cl=0.1 μm, the residual strain is 40.4×10^{-6}. It is shown in Fig. 2 that there are two branches: the stable branch and the unstable branch. The voltage of the intersection point (p) between the stable and unstable branches is pull-in voltage, V_{pl}; and the corresponding displacement is the pull-in displacement, w_{pl}. Noting that the unstable branch only exists theoretically, which cannot be measured in experiment. Therefore, the pull-in instability is also called a saddle–node bifurcation phenomenon.

3.2.2. Effect of Casimir force

In order to study the effect of Casimir force on the pull-in instability, the variations of the maximum nondimensional beam displacement with the applied voltage for clamped–clamped beam are plotted in Fig. 3, in which the results of the beam with Casimir force considered (blue line) are compared with those without Casimir force (red line). The geometrical and material properties are L=400 μm, b=100 μm, h=1 μm, d=0.2 μm, E=151 Gpa and ν=0.3, and Cl=0.1 μm, the residual stress is zero, fringing field parameter f=0. By studying the red line (Casimir force ignored), it reveals that the nondimensional displacement starts from zero and then increasing nonlinearly with applied voltage increases from zero; as the applied voltage reaches to the maximum voltage (pull-in voltage, V_{pl}), which corresponds to the maximum nondimensional displacement, w_{pl}, the nondimensional displacement will continue to increases and finally reaches to 1.0 with applied

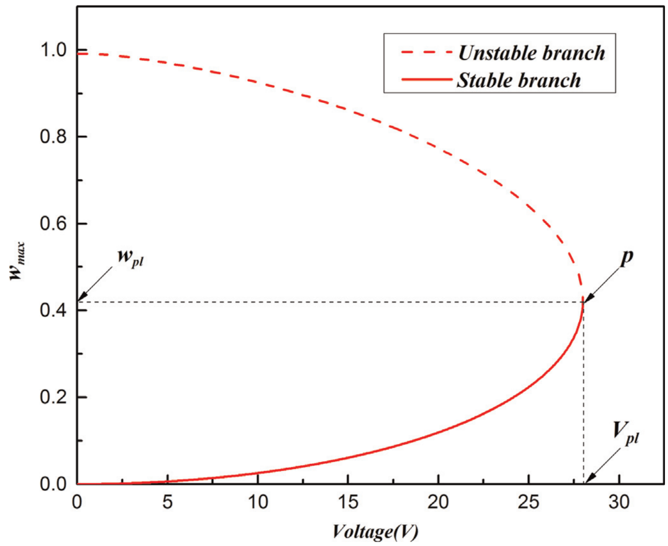

Fig. 2. Nondimensional displacement with applied voltage (the solid line is stable branch; dash line is unstable branch.).

voltage decreasing. However, with Casimir force considered as shown by the blue line, there is an initial w_0 although no voltage is applied on the beam, which is due to the Casimir force between the two electrodes. Besides, at the top of the unstable branch, residual displacement, w_r (< 1.0), is finally reached without voltage applied, where the Casimir force is just equal to the elastic restoring force of the beam theoretically. It is also shown in Fig. 3 that Casimir force not only reduces pull-in voltage from V_{pl1} to V_{pl2}, but also reduces pull-in displacement from w_{pl1} to w_{pl2}. All of these characteristics reveal that the effect of Casimir force on the system cannot be ignored.

3.2.3. The minimum gap and detachment length

As Casimir force is the spontaneous force between the flexible beam and substrate, the flexible beam will be driven to attach to the substrate if Casimir force (α_3 in Eq. (41)) reaches a critical value and without voltage applied, which is called the critical Casimir parameter α_{cr} as discussed in [1,26]. It is known from Eq. (42) that α_3 is associated with the beam length L and initial gap d between the two electrodes. Therefore, based on the parameters of system

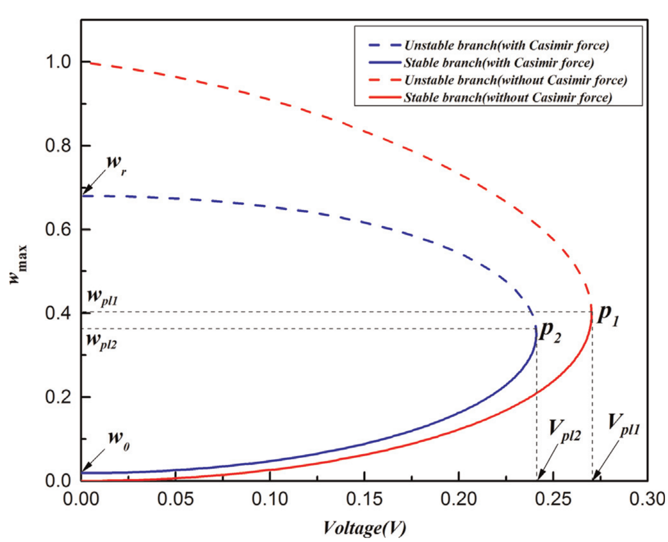

Fig. 3. Effect of Casimir force on the maximum displacement for $f_c = 0$ and $f_c \neq 0$. (For interpretation of the references to color in this figure legend, the reader is referred to the web version of this article.)

in Fig. 3, two cases are employed to study the pull-in instability: (I) only gap d changes and other parameters are kept as constants; (II) only length L changes and other parameters are kept as constants. For both cases, the variations of the maximum nondimensional displacement of the beam versus the applied voltage are depicted in Fig. 4(a and b), respectively. As shown in Fig. 4 (a) for case I, the pull-in voltage V_{pl} decreases as gap d decreases, which is reasonable because the Casimir force increases with gap decreasing. Moreover, the initial displacement w_0 increases and the residual displacement w_r decreases with gap d decreases. As gap d decrease to a critical value, d_{min}, the initial displacement w_0 is equal to the residual displacement w_r, i.e., $w_0 = w_r$. Such critical d_{min} is called the minimum gap [1]. In another words, the beam will collapse onto the substrate if the gap $d < d_{min}$ with other parameters fixed. For case II as plotted in Fig. 4(b), the pull-in voltage V_{pl} decreases as beam length L increases, which is almost the same with Fig. 4(a). Similarly, the initial displacement w_0 increases and the residual displacement w_r decreases with length L increases. Finally, the beam may collapse onto the substrate spontaneously without voltage applied when the length L increases to a critical value, L_{max}, where $w_0 = w_r$. Here, the maximum L_{max} is called the detachment length [28], which means the beam are no longer stable beyond this beam length with no voltage applied and other parameters fixed.

The minimum gap and detachment length are two significant parameters for microstructure designers. For example, in micro-/nano-resonators design, the designer should avoid such critical point in order to achieve stable motions; however, in switching applications the designer takes advantage of this effect to optimize the performance of the device.

By further considering clamped–clamped beam NEMS, the effect of the gap d on the parameter of Casimir force, pull-in voltage and pull-in displacement are plotted in Fig. 5. The geometrical and material parameters are $L/k = 2000$ nm, $b/k = 500$ nm, $h/k = 15$ nm, $E = 151$ Gpa and $\nu = 0.3$, $Cl = 0.1$ µm, $N = 0$ and $f = 0$, where k is a nondimensional size scale parameter. The results of three cases ($k = 0.2$, 0.5, 1.0) are presented for each plot, respectively.

It is evident in Fig. 5(a) that the parameter of Casimir force increases nonlinearly with gap decreasing. However, the curves are truncated below the minimum gap as the beam collapses onto the substrate beyond the minimum gap. It is interesting that the critical value α_{cr} corresponding to the minimum gap are same although the minimum gap are different for different k as shown in Fig. 5(a). It is also shown in Fig. 5(b) that the pull-in voltage decreases monotonically with gap decreasing and finally reduces to zero when gap is equal to the minimum gap. And the pull-in displacement is also decreases with gap decreasing as depicted in Fig. 5(c). Similarly, the curves are also truncated at the minimum gap, which is corresponding to the same minimum pull-in displacement w_{min}^{pl}, although size scale k is different.

Similar to the minimum gap, the detachment length is another design parameter for the nanostructure. Here, the effects of beam length on the parameter of Casimir force, pull-in voltage and pull-in displacement are studied as plotted in Fig. 6, where the parameters are $b/k = 500$ nm, $h/k = 15$ nm, $d/k = 10$ nm, $E = 151$ Gpa, $\nu = 0.3$, $Cl = 0.1$ µm, $N = 0$ and $f = 0$. The size scale k is also introduced here as did in Fig. 5, where the result of $k = 2/3$, 1, 3/2 are specially studied. It is shown in Fig. 6(a) that the Casimir force increases with beam length increasing and other parameters fixed. Of course, the length is truncated at a critical value, i.e., detachment length L_{max}, beyond which the beam collapse onto the substrate without voltage applied. Again here, it is interesting that the critical parameters of Casimir force α_{cr}, which are corresponding to the detachment length, are same even size scale k is different. Since beam length affects the Casimir force, it inevitably changes the pull-in voltage. The variation of pull-in voltage with beam

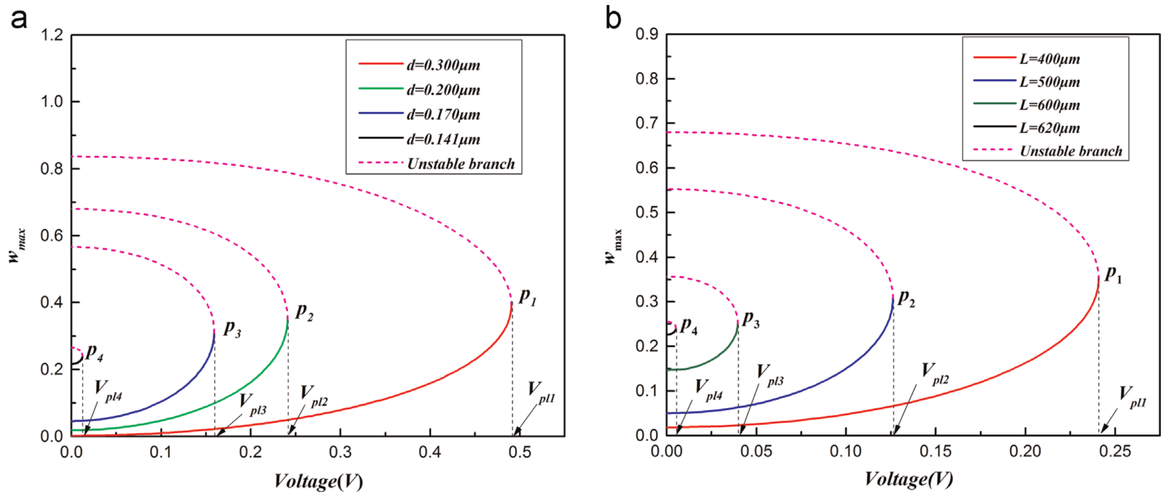

Fig. 4. The curves of w_{max} versus voltage for different gaps (a) and lengths (b).

length is presented in Fig. 6(b), where the results of different k are also plotted. It is evident that the pull-in voltage decreases with beam length increasing, and it reduces to zero when beam length is equal to detachment length, which means no voltage is needed for the beam pull-in instability. The nondimensional displacement is observed to decrease with beam length increasing. For different size scale k, as plotted in Fig. 6(c), the displacement reaches a minimum value, w_{min}^{pl}, when beam length increases to a critical value, detachment length L_{max}, which is same with the results in Fig. 5(c). From Figs. 5 and 6, it should be noted that some variables (e.g. α_{cr} and w_{min}^{pl}) are independent with the size scale. Is there any relationship between these variables and size scales? The size effect may play an important role in the characteristics in nanostructures, which will be discussed in the next section.

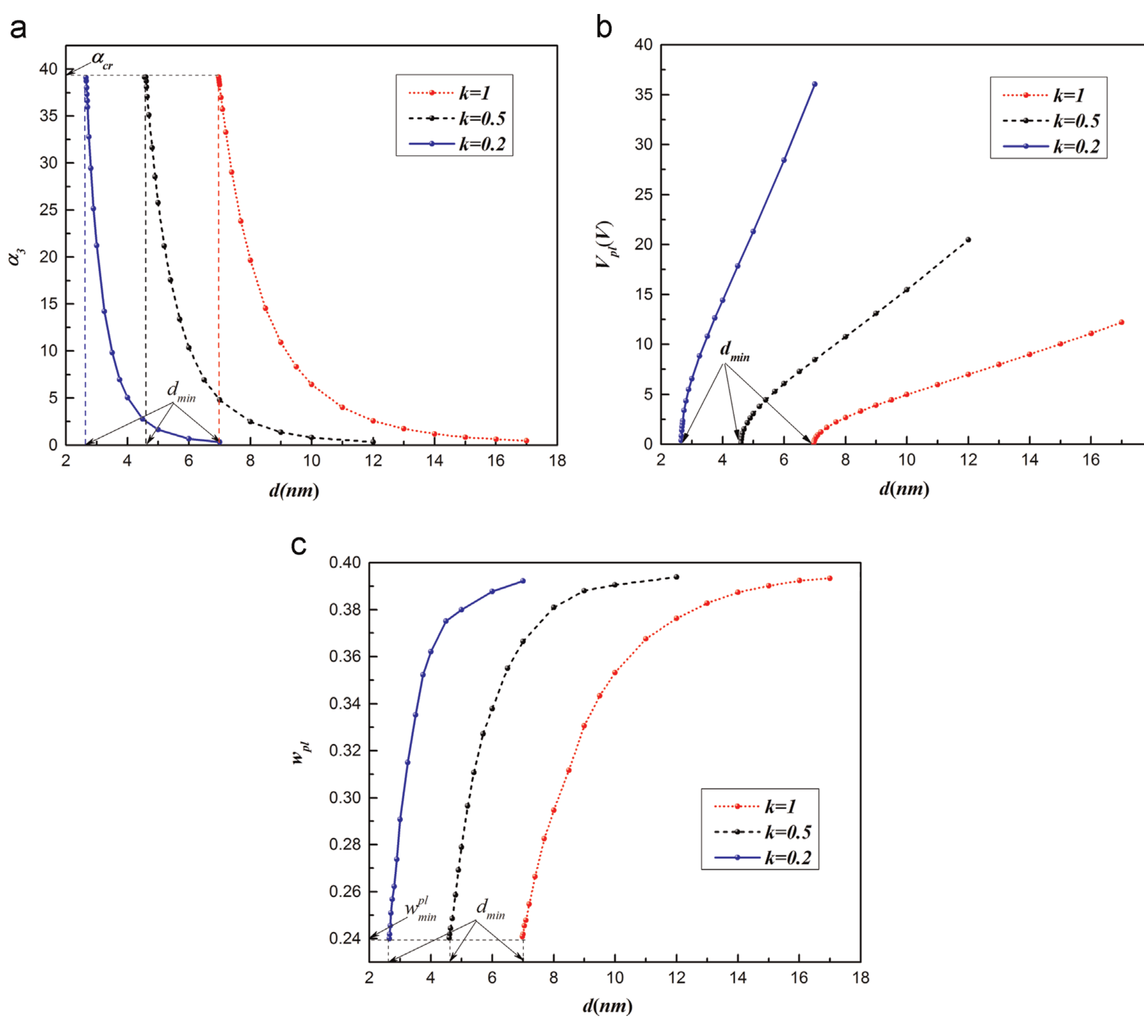

Fig. 5. The effect of gap on the Casimir force (a), pull-in voltage (b) and pull-in displacement (c) for different size scale k.

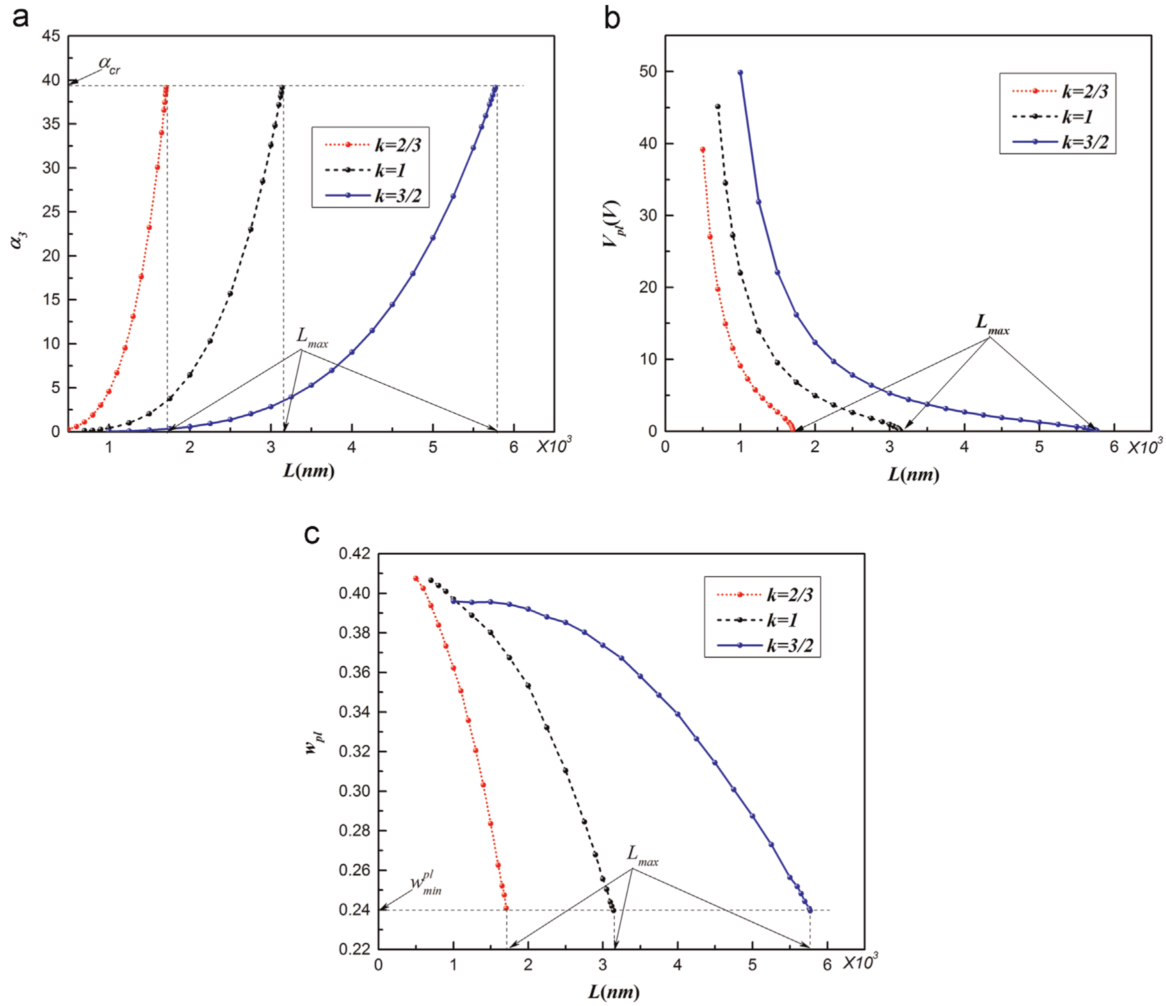

Fig. 6. The effect of beam length on the parameter of Casimir force (a), pull-in voltage (b) and pull-in displacement (c) for different size scale k.

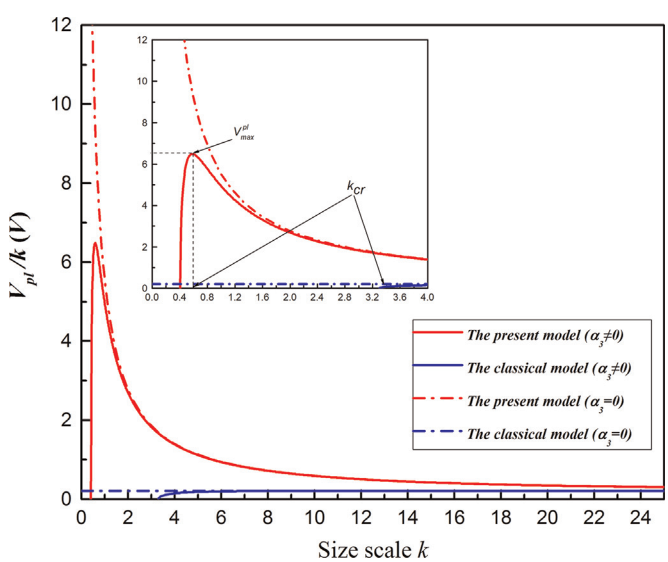

Fig. 7. The effect of size scale (k) on the normalized pull-in voltage (V_{pl}/k).

3.2.4. Size effect of the pull-in voltage

To study the size effect induced by strain gradient, the beam with parameters $L/k=2000$ nm, $b/k=500$ nm, $h/k=15$ nm, $d/k=10$ nm, $E=151$ Gpa, $\nu=0.3$ are studied, where k is size scale as defined above. The MLSP is taken to be $Cl=0.1$ μm. Thus, the variation of the size scale k indicates different structure sizes (while the beam shape is fixed). The results predicted by the present model (with size effect) are also compared with the corresponding ones by the modified couple stress model [13] and classical model (without size effect) as shown in Fig. 7.

For the present model, when Casimir force is ignored, the pull-in voltage increases with size scale decreasing, while the pull-in voltage increases firstly and then decreases sharply to zero with size scale decreasing when Casimir force is considered as shown in Fig. 7. There is a critical value, V^{pl}_{max}, which means the maximum normalized pull-in voltage no matter what size of the beam. It is evident that the pull-in voltage reduces to zero when the beam is small enough (k is very small), which indicates that the Casimir force should be considered in the model. For the classical model,

Table 1
Comparisons of the pull-in voltage from different models and the present model.

Data sources	V_{pl} /V
Experimental [44]	27.95
FIE [45]	28.24
DQM [46]	28.10
SGT [23]	28.02
The present model	27.99
Δ%	0.14%

Table 2
Comparisons of the results for different models.

Beam length V_{pl} in Ref.	L=250 μm Residual stress (Mpa)			L=350 μm Residual stress (Mpa)		
	0	100	−25	0	100	−25
[47] (MEMCAD)	40.10	57.60	33.60	20.30	35.80	13.70
[47] (2D)	39.50	56.90	33.70	20.20	35.40	13.80
[48] (GDQM)	39.13	57.62	33.63	20.36	35.99	13.60
[49] (2D-FEM)	39.56	57.35	33.50	20.19	35.71	13.42
[50] (Closed-form)	39.60	57.40	33.71	20.20	35.91	13.71
[45] (Analytical)	39.40	57.37	33.43	20.10	35.94	13.50
[51] (GM)	41.00	58.05	34.02	–	–	–
[52] (LMA)	40.38	58.87	34.12	20.60	36.77	13.63
Present model (a_3=0,f=0)	40.03	57.78	34.02	20.43	35.93	13.73
Present model (a_3=0,f≠0)	39.86	57.52	33.86	20.34	35.76	13.67
Present model (a_3≠0,f≠0)	39.86	57.52	33.86	20.34	35.76	13.67

on the other hand, the normalized pull-in voltage keeps constant when Casimir force is ignored, which is also pointed out in our previous papers [23,24]. Whereas the normalized pull-in voltage starts from zero, then increases gradually and finally converge to the same constant when Casimir force is included. For both models with Casimir force, external voltage is not needed for the beams whose size scale under the critical value, k_{cr}, because the existence of the Casimir force. In addition, when size scale k is very large, no matter what models and whether Casimir force included, the normalized pull-in voltage approach to the same value since the Casimir force and size effect are negligible for macro-scale structures.

3.2.5. Application of the present model

Finally the present model with Casimir force included is applied to predict the pull-in voltage of microbeam which is carried out experimentally [44]. The results are also compared with those from other models [23,45,46]. To be consistent with the experiment, the parameters of the fixed–fixed microbeam are set as L=210 μm, b=100 μm, h=1.5 μm, g=1.18 μm, the residual strain is 40.4×10^{-6} as shown in Table 1, where Rokin et al. [45] solved the problem by transforming the governing equation into the Fredholm Integral Euation (FIE), Kuang et al. [46] using the differential quadrature method (DQM) and Wang et al. [23] using the strain gradient theory (SGT) with Casimir force and fringing field ignored. Δ% is the percentage of difference between the present model and experimental result. The difference is only 0.14%, which is in good agreement with the experimental.

The present model is further applied to study the beams and compared the results with those available in literatures as given in Table 2, where the beams are clamped–clamped boundary conditions with varying beam length and residual stress. Other geometrical and material properties are b=50 μm, h=3 μm, d=1 μm, E=169 Gpa, ν=0.06 and Cl=0.1 μm. It is noted that α_3≠0 means the result with Casimir force included, while f≠0 means the result with fringe field included, respectively. The results from literatures are also shown, where the results obtained by Osterberg and Senturia [47] using micro-electro-mechanical computer aided design (MEMCAD), Sadeghian et al. [48] using GDQM, Haluzan et al. [49] using 2-D FEM, Chowdhury et al. [50] using a VLSI on-chip interconnect capacitance model, Sadeghian et al. [51] using the Galerkin methods and Pamidighantam et al. [52] using the LMA.

It is shown in Table 2 that the fringing field effect reduces the pull-in voltage, while it is found that, by contrasting the last two lines in the table, Casimir force does not significantly affect the pull-in voltage. This is due to Casimir force is effective in nanoscale, whereas it is very small at macro-scale and even be negligible at macro-scale.

4. Concluding remarks

By considering nonlinearities and Casimir force, a size-dependent model for electrostatically actuated nanobeam device is established based on the strain gradient elasticity theory and Hamilton principle. The governing equation together with boundary conditions is solved numerically with generalized differential quadrature (GDQ) method.

The results show that Casimir force can reduce the external applied voltage. Moreover, there exists a minimum gap between two electrodes and a maximum beam length (detachment length) where pull-in instability occurs without voltage applied. The size effect of the pull-in voltage is also discussed since the model incorporates strain gradient terms. In addition, comparisons are made between the results predicted from the present model with those of experimental data in literatures. Very good agreement is observed, which proves the new model is robust for describing the behavior of size-dependent pull-in instability for NEMS devices.

Acknowledgment

The work is supported by the National Natural Science Foundation of China (Grant nos. 11202117 and 11272186), Natural Science Fund of Shandong Province (ZR2012AM014), Opening fund of State Key Laboratory of Strength and Vibration of Mechanical Structures.

References

[1] J.-S. Duan, R. Rach, A pull-in parameter analysis for the cantilever NEMS actuator model including surface energy, fringing field and Casimir effects, Int. J. Solids Struct. 50 (2013) 3511–3518.
[2] J. Yang, X.L. Jia, S. Kitipornchai, Pull-in instability of nano-switches using nonlocal elasticity theory, J. Phys. D: Appl. Phys. 41 (2008) 035103 (8 pp.).
[3] M. Rasekh, S.E. Khadem, Pull-in analysis of an electrostatically actuated nano-cantilever beam with nonlinearity in curvature and inertia, Int. J. Mech. Sci. 53 (2011) 108–115.
[4] Y. Zhang, Y.P. Zhao, Numerical and analytical study on the pull-in instability of micro-structure under electrostatic loading, Sens. Actuator A: Phys. 127 (2006) 366–380.
[5] W.D. Nix, Mechanical-properties of thin-films, Metall. Trans. A: Phys. Metall.

Mater. Sci. 20 (1989) 2217–2245.
[6] W.J. Poole, M.F. Ashby, N.A. Fleck, Micro-hardness of annealed and work-hardened copper polycrystals, Scr. Mater. 34 (1996) 559–564.
[7] I. Vardoulakis, G. Exadaktylos, S.K. Kourkoulis, Bending of marble with intrinsic length scales: a gradient theory with surface energy and size effects, J. Phys. IV 8 (1998) 399–406.
[8] D.C.C. Lam, F. Yang, A.C.M. Chong, J. Wang, P. Tong, Experiments and theory in strain gradient elasticity, J. Mech. Phys. Solids 51 (2003) 1477–1508.
[9] A.W. McFarland, J.S. Colton, Role of material microstructure in plate stiffness with relevance to microcantilever sensors, J. Micromech. Microeng. 15 (2005) 1060–1067.
[10] E.C. Aifantis, Exploring the applicability of gradient elasticity to certain micro/nano reliability problems, Microsyst. Technol.: Micro- Nanosyst.-Inf. Storage Process. Syst. 15 (2009) 109–115.
[11] A.C. Eringen, On differential-equations of nonlocal elasticity and solutions of screw dislocation and surface-waves, J. Appl. Phys. 54 (1983) 4703–4710.
[12] M.E. Gurtin, A.I. Murdoch, A continuum theory of elastic material surfaces, Arch. Ration. Mech. Anal. 57 (1975) 291–323.
[13] F. Yang, A.C.M. Chong, D.C.C. Lam, P. Tong, Couple stress based strain gradient theory for elasticity, Int. J. Solids Struct. 39 (2002) 2731–2743.
[14] A. Assadi, Size dependent forced vibration of nanoplates with consideration of surface effects, Appl. Math. Model. 37 (2013) 3575–3588.
[15] S.L. Kong, S.J. Zhou, Z.F. Nie, K. Wang, The size-dependent natural frequency of Bernoulli–Euler micro-beams, Int. J. Eng. Sci. 46 (2008) 427–437.
[16] H.M. Ma, X.L. Gao, J.N. Reddy, A microstructure-dependent Timoshenko beam model based on a modified couple stress theory, J. Mech. Phys. Solids 56 (2008) 3379–3391.
[17] H.M. Ma, X.L. Gao, J.N. Reddy, A nonclassical Reddy–Levinson beam model based on a modified couple stress theory, Int. J. Multiscale Comput. Eng. 8 (2010) 167–180.
[18] S.L. Kong, S.J. Zhou, Z.F. Nie, K. Wang, Static and dynamic analysis of micro beams based on strain gradient elasticity theory, Int. J. Eng. Sci. 47 (2009) 487–498.
[19] J. Zhao, S. Zhou, B. Wang, X. Wang, Nonlinear microbeam model based on strain gradient theory, Appl. Math. Model. 36 (2012) 2674–2686.
[20] B. Wang, J. Zhao, S. Zhou, A micro scale Timoshenko beam model based on strain gradient elasticity theory, Eur. J. Mech.: A/Solids 29 (2010) 591–599.
[21] M. Asghari, M.H. Kahrobaiyan, M.T. Ahmadian, A nonlinear Timoshenko beam formulation based on the modified couple stress theory, Int. J. Eng. Sci. 48 (2010) 1749–1761.
[22] B. Wang, M. Liu, J. Zhao, S. Zhou, A size-dependent Reddy–Levinson beam model based on a strain gradient elasticity theory, Meccanica 49 (2014) 1427–1441.
[23] B.L. Wang, S.J. Zhou, J.F. Zhao, X. Chen, Size-dependent pull-in instability of electrostatically actuated microbeam-based MEMS, J. Micromech. Microeng. 21 (2011) 027001 (6 pp.).
[24] B. Wang, S. Zhou, J. Zhao, X. Chen, Pull-in instability analysis of electrostatically actuated microplate with rectangular shape, Int. J. Precis. Eng. Manuf. 12 (2011) 1085–1094.
[25] B. Wang, S. Zhou, J. Zhao, X. Chen, Pull-in instability of circular plate MEMS: a new model based on strain gradient elasticity theory, Int. J. Appl. Mech. 4 (2012) 1250003 (12 pp.).
[26] R.C. Batra, M. Porfiri, D. Spinello, Effects of Casimir force on pull-in instability in micromembranes, EPl 77 (2007) 20010 (6 pp.).
[27] W.-H. Lin, Y.-P. Zhao, Nonlinear behavior for nanoscale electrostatic actuators with Casimir force, Chaos Solitons Fractals 23 (2005) 1777–1785.
[28] W.H. Lin, Y.P. Zhao, Dynamic behaviour of nanoscale electrostatic actuators, Chin. Phys. Lett. 20 (2003) 2070–2073.
[29] R.C. Batra, M. Porfiri, D. Spinello, Vibrations and pull-in instabilities of microelectromechanical von Karman elliptic plates incorporating the Casimir force, J. Sound Vib. 315 (2008) 939–960.
[30] R.C. Batra, M. Porfiri, D. Spinello, Reduced-order models for microelectromechanical rectangular and circular plates incorporating the Casimir force, Int. J. Solids Struct. 45 (2008) 3558–3583.
[31] W.H. Lin, Y.P. Zhao, Casimir effect on the pull-in parameters of nanometer switches, Microsyst. Technol. 11 (2005) 80–85.
[32] Y.-G. Wang, W.-H. Lin, X.-M. Li, Z.-J. Feng, Bending and vibration of an electrostatically actuated circular microplate in presence of Casimir force, Appl. Math. Model. 35 (2011) 2348–2357.
[33] X.L. Jia, J. Yang, S. Kitipornchai, Pull-in instability of geometrically nonlinear micro-switches under electrostatic and Casimir forces, Acta Mech. 218 (2011) 161–174.
[34] C.L. Dym, I.H. Shames, Solid Mechanics: A Variational Approach, McGraw-Hill Inc., New York, 1973.
[35] M. Rahaeifard, M.H. Kahrobaiyan, M.T. Ahmadian, K. Firoozbakhsh, Size-dependent pull-in phenomena in nonlinear microbridges, Int. J. Mech. Sci. 54 (2012) 306–310.
[36] M.I. Younis, E.M. Abdel-Rahman, A. Nayfeh, A reduced-order model for electrically actuated microbeam-based MEMS, J. Microelectromech. Syst. 12 (2003) 672–680.
[37] C. Shu, B.E. Richards, Parallel simulation of incompressible viscous flows by generalized differential quadrature, Comput. Syst. Eng 3 (1992) 11.
[38] C. Shu, C.M. Wang, Treatment of mixed and nonuniform boundary conditions in GDQ vibration analysis of rectangular plates, Eng. Struct. 21 (1999) 125–134.
[39] J.R. Quan, C.T. Chang, New insights in solving distributed system equations by the quadrature method.1. Analysis, Comput. Chem. Eng. 13 (1989) 779–788.
[40] J.R. Quan, C.T. Chang, New insights in solving distributed system equations by the quadrature method 2. Numerical experiments, Comput. Chem. Eng. 13 (1989) 1017–1024.
[41] W. Chen, T. Zhong, The study on the nonlinear computations of the DQ and DC methods, J. Numer. Method Partial Differ. Equ. 13 (1997) 19.
[42] S. Tomasiello, Differential quadrature method: application to initial-boundary-value problems, J. Sound Vib. 218 (1998) 573–585.
[43] A.H. Nayfeh, B. Balachandran, Applied Nonlinear Dynamics, Wiley, New York, 1995.
[44] H.A.C. Tilmans, R. Legtenberg, Electrostatically driven vacuum-encapsulated polysilicon resonators. 2. Theory and performance, Sens. Actuator A: Phys. 45 (1994) 67–84.
[45] H. Rokni, R.J. Seethaler, A.S. Milani, S. Hosseini-Hashemi, X.-F. Li, Analytical closed-form solutions for size-dependent static pull-in behavior in electrostatic micro-actuators via Fredholm integral equation, Sens. Actuators A: Phys. 190 (2013) 32–43.
[46] J.H. Kuang, C.J. Chen, Dynamic characteristics of shaped micro-actuators solved using the differential quadrature method, J. Micromech. Microeng. 14 (2004) 647–655.
[47] P.M. Osterberg, S.D. Senturia, M-TEST: a test chip for MEMS material property measurement using electrostatically actuated test structures, J. Microelectromech. Syst. 6 (1997) 107–118.
[48] H. Sadeghian, G. Rezazadeh, P.M. Osterberg, Application of the generalized differential quadrature method to the study of pull-in phenomena of MEMS switches, J. Microelectromech. Syst. 16 (2007) 1334–1340.
[49] D.T. Haluzan, D.M. Klymyshyn, S. Achenbach, M. Boerner, Reducing pull-in voltage by adjusting gap shape in electrostatically actuated cantilever and fixed–fixed beams, Micromachines 1 (2010) 68–81.
[50] S. Chowdhury, M. Ahmadi, W.C. Miller, A closed-form model for the pull-in voltage of electrostatically actuated cantilever beams, J. Micromech. Microeng. 15 (2005) 756–763.
[51] H. Sadeghian, G. Rezazadeh, Comparison of generalized differential quadrature and Galerkin methods for the analysis of micro-electro-mechanical coupled systems, Commun. Nonlinear Sci. Numer. Simul. 14 (2009) 2807–2816.
[52] S. Pamidighantam, R. Puers, K. Baert, H.A.C. Tilmans, Pull-in voltage analysis of electrostatically actuated beam structures with fixed–fixed and fixed-free end conditions, J. Micromech. Microeng. 12 (2002) 458–464.